

Biomimetic magnetic nanoparticles

by Michael T. Klem^{1,2,3}, Mark Young^{2,3,4}, and Trevor Douglas^{1,2,3*}

Magnetic nanoparticles are of considerable interest because of their potential use in high-density memory devices, spintronics, and applications in diagnostic medicine. The conditions for synthesis of these materials are often complicated by their high reaction temperatures, costly reagents, and post-processing requirements. Practical applications of magnetic nanoparticles will require the development of alternate synthetic strategies that can overcome these impediments. Biomimetic approaches to materials chemistry have provided a new avenue for the synthesis and assembly of magnetic nanomaterials that has great potential for overcoming these obstacles.

There is growing interest in materials chemistry for taking advantage of the physical and chemical properties of biomolecules in the development of the next generation of nanoscale materials. In particular, researchers are beginning to mimic biological systems in achieving molecular-level control via self-assembly and directed assembly processes. A biomimetic approach to materials synthesis offers the possibility of controlling size, shape, crystal structure, orientation, and organization. This approach has been used successfully in the synthesis of magnetic materials ranging from ferrimagnetic Fe_3O_4 (as found in magnetotactic bacteria) to hard magnetic alloys (such as the L1_0 phases of FePt and CoPt). There is little doubt that such bioinspired pathways will prove useful in the development of the next generation of novel materials.

Within the largely diamagnetic background of biological systems, there are a few examples of ferrimagnetic materials that have inspired a generation of materials scientists. The single-domain magnetic materials synthesized by magnetotactic bacteria^{1,2}, the apparent transformation of antiferromagnetic iron oxide phases to magnetite in chiton teeth^{3,4}, and the ferrihydrite mineral core of ferritin are examples of biologically produced magnetic materials with unique properties⁵. In general, biomineralization illustrates the exquisite level of control over composition, polymorph selection, orientation, and morphology that can be achieved under mild reaction conditions. The goal of biomimetic

¹Department of Chemistry and Biochemistry, Montana State University, Bozeman, MT 59717, USA

²Center for Bioinspired Materials, Montana State University, Bozeman, MT 59717, USA

³Thermal Biology Institute, Montana State University, Bozeman, MT 59717, USA

⁴Department of Plant Sciences, Montana State University, Bozeman, MT 59717, USA

*E-mail: tdouglas@chemistry.montana.edu

materials chemistry is to use our understanding of fundamental biomineralization processes to synthesize target materials that incorporate specific properties by design⁶. To this end, great progress has been made in the control that can be exerted over magnetic materials synthesis using protein/mineral interfaces as templates for directed synthesis. In particular, the use of phage display for the identification of specific peptide sequences with a high affinity for specific material polymorphs and the use of protein architectures to control morphology have generated a truly biomimetic approach to synthesis of materials well beyond the bounds of biology. Here, we outline the formation and characterization of some important bio- and bioinspired magnetic materials.

Magnetotactic bacteria

Magnetotactic bacteria contain intracellularly produced crystals² of magnetite (Fe_3O_4) and/or greigite (Fe_3S_4). The novel structures of the magnetite material contained inside the bacteria have been under active study since their initial discovery, partly because they represent a mild form of renewable synthesis for an interesting class of magnetic nanostructures^{2,7-18}. The mineralization processes are highly regulated, resulting in the formation of uniform magnetic nanoparticles that are single domain and show species-specific morphology. Within the bacteria, the magnetic particles are aligned in single or multiple chains parallel to the cell axis (Fig. 1). Each particle possesses a magnetic moment, and magnetic interactions between particles in a chain are oriented along the chain¹⁹. This allows the cell to have a large magnetic moment and, thus, enables the bacterium to sense and migrate along geomagnetic field lines, maintaining its position within the interface of the oxic-anoxic zone (the transition region in water at the interface between oxidizing and reducing environments)²⁰.

The chains consist of individual magnetite crystals that are combinations of the {111} (octahedron) and {100} (cubic) forms. The [111] easy axis of magnetization in the crystals are primarily parallel to the chain axis²¹. The magnetic nanoparticles and the associated phospholipid vesicle are collectively termed the magnetosome. When magnetosomes are arranged in a single chain, as in *Magnetospirillum magnetotacticum*, a permanent magnetic moment is present that has a remanent magnetization approaching saturation (0.603 T)¹⁹. A chain of 20 magnetosomes with a volume of 50 nm^3 each would have a magnetic moment of

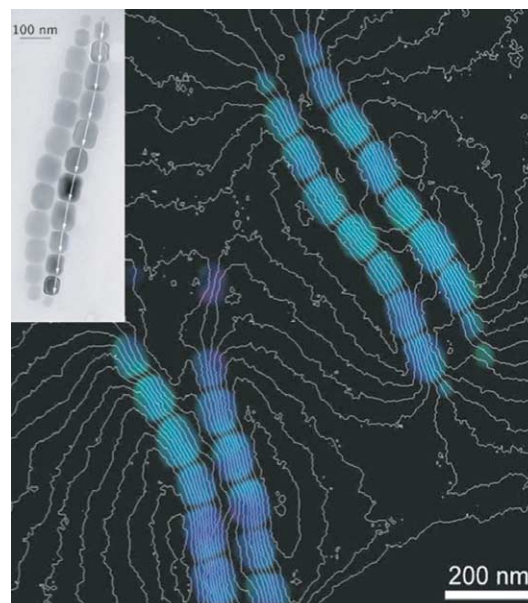


Fig. 1 Representative electron hologram of two double chains of magnetite in a single magnetotactic bacteria isolated from a stream in Hungary. The magnetic field lines are oriented so that the vector points toward the northwest in the image. Inset: a typical bright-field image of one of the double chains. (Reprinted with permission from¹⁷⁵. © 2005 Institute of Physics.)

approximately $1 \times 10^{-15} \text{ A m}^2$, which is sufficient to orientate the moment along the geomagnetic field at ambient temperatures¹. This value is also consistent with results from electron holography ($5 \times 10^{-16} \text{ A m}^2$, Fig. 1)¹⁵.

The characteristics exhibited by magnetite crystals appear to be consistent within a given species, with some variations within a single magnetosome chain^{22,23}. Many crystals of this type have been studied by high-resolution electron microscopy and/or selected-area electron diffraction, and idealized crystal characteristics, based on a combination of symmetry-related crystal faces, have been proposed²². The morphology has been used as an indication of the biological origin of nanoscale magnetite crystals²⁴. In addition to the approximate equidimensional crystal shapes seen in *Magnetospirillum magnetotacticum*, nonequidimensional shapes have been described for other species²⁵. Crystals that have elongated, prismatic-like characteristics, corresponding to the anisotropic growth of symmetry-related faces, could occur because of anisotropy in either the growth environment (e.g. concentration gradients) or the growth site²⁶. In the case of nonequidimensional magnetosomes, anisotropy in the environment could arise from either differences in the flux of ions through the magnetosome membrane surrounding the crystal or the anisotropic interactions between the magnetosome membrane and the growing crystal²⁶⁻²⁸.

Ferritin: a model system

Ferritins form a class of proteins that are ubiquitous in all domains of life^{29,30}. There are subtle differences between prokaryotic, eukaryotic, and archaeal ferritins, but they share much structural similarity. Ferritins consist of 24 protein subunits that self-assemble into a cage-like architecture in which a hydrated ferric oxide/phosphate is mineralized.

Mammalian ferritins consist of a mixture of two different types of subunits. These are known as heavy (H) and light (L) chains based on relative electrophoretic mobilities. Ratios of H to L chain subunits are found to vary between organisms, as well as between tissues within an organism³¹.

Structurally, the two types of subunit are similar. Each is composed of a four-helix bundle capped by a fifth helical domain that lies at $\sim 60^\circ$ to the bundle axis (Fig. 2A). In the quaternary structure, the subunits are aligned in 12 sets of antiparallel pairs, which gives rise to a roughly rhombic dodecahedron shape. Subunit interactions lead to a packed shell with channels of $\sim 3 \text{ \AA}$ in diameter at the three- and four-fold symmetry axes (Fig. 2B). The three-fold channels are primarily hydrophilic and lined with aspartate and glutamate residues. In contrast, the four-fold channels are surrounded by four helices (from differing subunits) and are largely hydrophobic³².

The role of ferritin *in vivo* is to sequester Fe as a hydrated form of iron oxide (or phosphate), predominantly as the mineral ferrihydrite. The magnetic properties of this mineral have been studied extensively^{5,33-36}. Ferrihydrite is a hydrous iron oxide that is antiferromagnetically ordered at low temperature. The blocking temperature of this composite material is $\sim 15 \text{ K}$, below which hysteresis from the uncompensated moments is observed. The cores of

mammalian ferritins appear to be crystalline, and high-resolution electron microscopy reveals either single crystals or small crystalline domains interspersed with some iron oxide of low crystallinity³⁷. Electron diffraction patterns obtained from mammalian ferritin cores typically exhibit five or six diffraction lines attributed to ferrihydrite^{37,38}.

The ferrihydrite cores of mammalian ferritins usually have just small amounts of inorganic phosphate. However, while ferritins from marine mollusks (limpets and chitons) also contain small amounts of phosphate, their cores are of poor crystallinity³⁹. On the other hand, bacterial ferritin cores have been shown to contain so much phosphate that they are essentially iron(III) phosphate with a small amount of iron oxyhydroxide. These cores exhibit no discernable electron diffraction and their magnetic properties indicate weakened exchange interactions as a result of the replacement of O bridges by PO_4^{3-} leading to a less efficient magnetic superexchange between the metal sites^{37,40,41}.

The mineralization of ferrihydrite within ferritin is a multistep process involving Fe(II) oxidation, hydrolysis, nucleation, and crystal growth. Fe(II) ions pass into the cavity of the protein through the hydrophilic three-fold channels. In human ferritin, metal-binding sites present on H-chain subunits but absent in L-chain subunits have been identified as the ferroxidase center, which catalyzes the oxidation of Fe(II) to Fe(III)^{42,43}. Site-directed mutagenesis at the ferroxidase site of the H-chain subunits results in reduced rates of mineralization⁴³. Glutamic acid residues on the interior ferritin surface are believed to aid the nucleation process⁴³. Proteins with mutations that disrupt both the ferroxidase and nucleation sites show a loss of spatial control in the mineralization reaction⁴³.

Calculations to determine the electrostatic potential of ferritin, using the human H-chain homopolymer (HuHF), reveal novel aspects of the protein⁴⁴. The calculated charge density correlates well with regions previously identified as active sites within the protein cage. The three-fold channels, ferroxidase sites, and nucleation sites all show the expected negative electrostatic potential values. However, the outer entrance to the three-fold channel is surrounded by regions of positive potential, creating an electrostatic gradient directed toward the interior cavity. This electrostatic gradient provides a guidance mechanism for cations entering the protein cavity, suggesting that the three-fold channel is the major entrance to the protein^{29,30}.

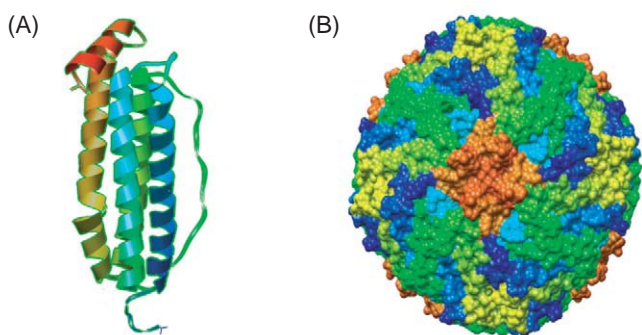


Fig. 2 (A) Subunit conformation of mammalian ferritin, showing four-helix bundle with a shorter helix at $\sim 60^\circ$ to the bundle axis and a 17-residue loop on the left. (B) Surface-rendered view of the mammalian ferritin quaternary structure, looking down four-fold axis.

The stoichiometry of Fe oxidation by O₂ has been shown to depend on Fe/protein ratio⁴⁵. At low levels of Fe (≈ 24 Fe(II)/protein), the stoichiometry follows eq 1, with H₂O₂ and ferrihydrite as the products. At high Fe(II) levels (>240 Fe(II)/protein), the stoichiometry follows eq 2. The mechanistic process of core formation appears to have two components⁴⁶. At low levels of Fe loading, the ferroxidase activity of the H-chain subunit dominates according to eq 1. At higher levels of loading Fe, however, the expanding mineral surface catalyzes the oxidation reaction according to eq 2.



DeminerIALIZED ferritin (apoferritin) is a hollow, spherical protein shell homogeneously dispersed in aqueous media. For mineralization to occur within the confines of the protein rather than in the bulk solution, the system is biased so that reaction inside the protein shell is favored over reaction outside the protein. There are clear instances in the case of ferritin where protein-assisted mineralization occurs, making mineralization inside the protein cage faster than bulk precipitation. This discrimination between inside and outside is crucial to the effective functioning of the protein *in vivo*. It is also central to a synthetic approach for forming nanophase materials within the ferritin protein shell⁴⁷.

Ferritin in magnetic nanoparticle synthesis

The ferrimagnetic iron oxide phase Fe₃O₄ synthesized within ferritin protein has become known as 'magnetoferritin'^{5,33,48-52}. The synthesis of magnetoferritin is carried out anaerobically under Ar or N₂ at elevated temperature (60–65°C) and pH (8.5) by the stepwise addition of Fe(II) to a solution of apoferritin, followed by partial oxidation (Fig. 3). The reaction product is a homogeneous black-brown solution, compared to the blood-red color of native ferritin, which can be precipitated by high magnetic fields. Control experiments using 0.1 M NaCl in place of apoferritin produced a black, extensively aggregated precipitate of magnetite (Fe₃O₄).

Magnetoferritin cores imaged by transmission electron microscopy reveal an homogeneous size distribution with an average particle diameter of 7.3 nm, commensurate with the interior diameter of the protein cage (Table 1, Figs. 4A and 4B).

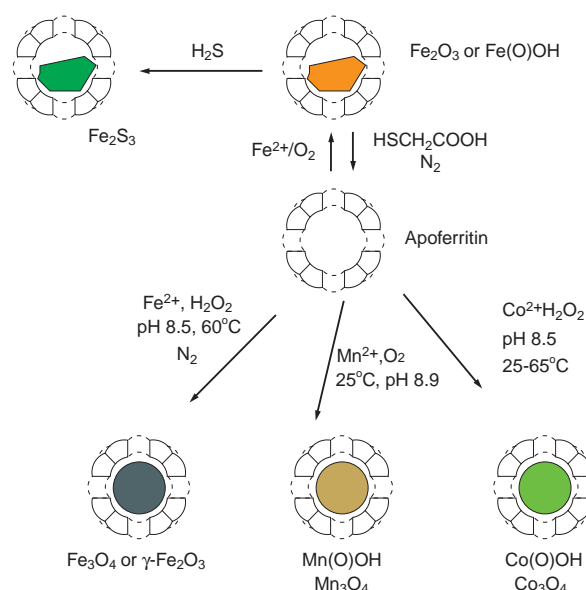


Fig. 3 Some of the synthetic pathways that are possible using ferritin as a constrained reaction environment.

Electron diffraction confirms a face-centered cubic mineral structure. However, from the data, it was not possible to distinguish between magnetite (Fe₃O₄) and its oxidation product, maghemite (γ -Fe₂O₃). Dynamic light scattering and polyacrylamide gel electrophoresis show no perturbation in the exterior diameter of the protein cage or its mobility (i.e. the distance travelled in the gel electrophoresis experiments) with respect to apoferritin.

The magnetic characterization of magnetoferritin is well established^{5,49-55}. Field-dependent magnetization studies of magnetoferritin do not demonstrate hysteresis at 300K but do at lower temperature, which is consistent with superparamagnetic behavior (Figs. 4C and 4D)^{48,51}. Fitting the data to a Langevin function indicates roughly 13 100 Bohr magnetons (μ_B) per molecule, corresponding to a particle of 8.5 nm diameter containing on the order of

Table 1 Interior and exterior diameters of various protein cages.

Protein cage	Interior diameter (nm)	Exterior diameter (nm)
Horse spleen ferritin	8	12
Dps from <i>L. innocua</i>	6	9
Cowpea chlorotic mottle virus (CCMV)	24	28
subE CCMV mutant	24	28
sHsp from <i>M. jannaschii</i>	8	12
Lumazine synthase from <i>B. subtilis</i>	8	15
Tobacco mosaic virus	4	18

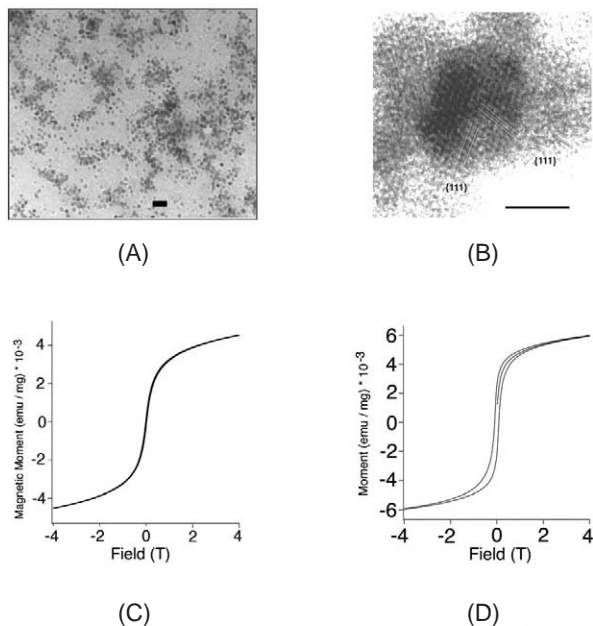


Fig. 4 (A) Transmission electron micrograph (TEM) of magnetite (Fe_3O_4) synthesized in the protein cage ferritin. Scale bar is 40 nm. (B) High-resolution TEM of a single magnetoferritin core with the {111} lattice fringes indicated. Scale bar is 4 nm. (C) Hysteresis loop (magnetic moment versus field) of magnetoferritin at room temperature. Superparamagnetic behavior of ensemble is indicated by the absence of any coercive field. (D) Hysteresis loop of magnetoferritin at 4 K with a coercive field of ~ 1200 G.

12 000 Fe atoms. Modifications of the Langevin function have also been used to obtain better fits to the observed data⁵⁴. Deconvolution of the anisotropy energy density, as determined by alternating current magnetic susceptibility (ACMS), suggests that, for a loading factor of 1000 Fe atoms per assembled protein cage, the average magnetic particle size is 6.5 nm⁵⁶. Comparisons of the anisotropy energies and blocking temperatures of Fe_3O_4 in various protein cages are given in Table 2.

The ^{57}Fe Mössbauer spectrum of magnetoferritin has been measured in both the presence and the absence of an applied magnetic field⁵¹. The zero-field Mössbauer spectrum is different from native ferritin and has line shapes consistent with Fe_3O_4 or $\gamma\text{-Fe}_2\text{O}_3$. However, in the presence of a 9 T

Table 2 Comparison of blocking temperature and anisotropy energies for Fe_3O_4 in various protein cages.

Cage	Anisotropy energy (10^{-23} J)	Average blocking temperature (K)
Dps from <i>L. innocua</i>	99	5
Horse spleen ferritin	618	30
Cowpea chlorotic mottle virus (CCMV)	4933	200

field, the spectrum resembles that of maghemite ($\gamma\text{-Fe}_2\text{O}_3$) more than that of magnetite (Fe_3O_4).

Even though ferritins have evolved to sequester Fe *in vivo*, synthetic reactions with metal ions other than Fe(II) result in the formation of cores exclusively within the protein cage (Fig. 3). Thus, Mn(II) undergoes air oxidation and mineralization to form Mn(O)OH and Mn_3O_4 within the cage⁵⁷⁻⁵⁹. Co(II) also undergoes oxidation with H_2O_2 to form a Co(O)OH mineral⁶⁰ and, under appropriate conditions (pH = 8.5 and 65°C), the antiferromagnetic spinel phase Co_3O_4 is formed within the protein cage.

ACMS measurements on Co_3O_4 in ferritin have determined a blocking temperature of ~ 4 K and give an average anisotropy energy density of $(1.2 \pm 0.2) \times 10^4$ J/m³. The real part of the ac susceptibility data fits well to a Curie-Weiss law, suggesting an interaction that favors parallel alignment of the magnetic moment between particles with a critical ordering temperature of 4.8 ± 0.4 K. Vibrating sample magnetometry measurements reveal a Néel temperature of 20 K (bulk is 40 K), using both the extracted magnetic saturations and linear susceptibilities. Hysteresis is also observed in the sample at 2 K, with a coercive field of 140 G. The uncompensated spins that make up the net magnetic moments have been determined to be restricted mostly to the surface of the particles⁶¹.

A range of other closed-shell protein architectures has been used to constrain the synthesis of magnetic nanoparticles. These include a class of ferritin-like proteins known as Dps (DNA-binding proteins from starved cells)⁶², the cowpea chlorotic mottle virus (CCMV), a small heat-shock protein (sHsp), lumazine synthase, and tobacco mosaic virus (TMV).

Dps proteins

The Dps family of proteins represent smaller size-constrained supramolecular cage structures that are capable of similar mineral entrapment to that seen in ferritin. The Dps cages have an architecture comprising just 12 subunits (Fig. 5). Like ferritins, the Dps protein isolated from the gram-positive bacterium *Listeria innocua* contains a ferroxidase center. Although it lacks sequence homology with mammalian ferritins, it does have similar structural motifs⁶³⁻⁶⁶. The *Listeria* Dps has an exterior diameter of 9.0 nm and an interior diameter of 6 nm (Table 1), and can contain a mineral core of iron oxide. Constrained magnetic nanoparticle

mineralization has been achieved in *Listeria Dps*. Controlled Fe oxidation at elevated temperature (65°C) and pH (8.5) results in the formation of nanoparticles of ferrimagnetic Fe₃O₄⁶⁷. Iron oxide mineralized samples investigated by electron microscopy reveal a narrow size distribution of 4.5–6.0 nm for a mineral core comprising, on average, 500 Fe atoms per cage^{65,68}. Substitution of Co(II) for Fe(II) in this reaction results in the formation of Co₃O₄⁶⁹. The average blocking temperature of the 3.5 nm noninteracting ferrimagnetic Fe₃O₄ particles determined by ACMS is 5 K with a coercive field of 200 G at 5 K⁵⁵. The effective anisotropy energy density is 0.04 J/cm³ compared with 0.02 J/cm³ for the bulk phase because of the contribution of surface spins arising from the small particle size⁵⁵. The Co₃O₄ nanoparticles also show hysteresis from uncompensated moments at 5.5 K, with a coercive field of 400 G and a saturated magnetization of 3.7 A m²/mg⁷⁰.

Cowpea chlorotic mottle virus (CCMV)

CCMV is an RNA-containing plant virus. The quaternary structure is icosahedral, and the cage-like structure is approximately 28 nm in outside diameter (Table 1, Fig. 5). The virions contain 180 identical coat protein subunits (19.8 kDa each) that self-assemble to form a protein cage 2–4 nm thick and with a central cavity (5.5 × 10⁶ Å³) in which the viral RNA is packaged⁷¹.

The crystallization of guest molecules inside CCMV can be achieved because the wild-type virion provides a positively charged interior interface, which facilitates the aggregation and crystallization of ions. The virus has been shown to be a good system for the crystallization and growth of polyoxometalate species (e.g. vanadate, molybdate, and tungstate)⁷². To test the role of electrostatic effects in directing the mineralization, a genetic mutant of CCMV was constructed (subE) in which all the basic residues on the N-terminus of the coat protein were substituted for glutamic acids (E), thus dramatically altering the electrostatic character of the interior surface of the assembled protein cage⁷³.

The subE mutant is able to catalyze the oxidative hydrolysis of Fe(II) to form an iron oxide nanoparticle (lepidocrocite) within the interior of the protein cage. The nanomaterial within the cage is both size- and shape-constrained by the interior dimensions of the particle. Wild-type CCMV, on the other hand, demonstrated no spatially defined catalytic activity when it was incubated in the presence of Fe(II).

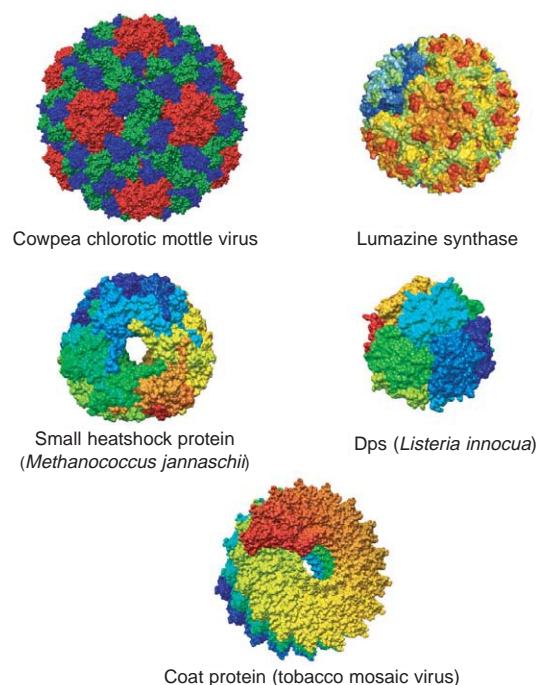


Fig. 5 Surface-rendered view of the quaternary structures of protein cages that are useful in the synthesis of constrained magnetic materials.

Instead, bulk autoxidation and hydrolysis was observed, but no virion-encapsulated mineral was detected. Thus, selective engineering of the virion is possible, illustrating the plasticity of these architectures as biotemplates.

While subE has been used as a constrained reaction environment for the mineralization of lepidocrocite, it has not yet been used for making ferrimagnetic particles of maghemite (γ -Fe₂O₃) since the mutant is not stable under the conditions necessary for synthesizing the magnetic mineral. SubE can, however, be stabilized to these conditions by crosslinking the protein cage's subunits with a bifunctional cross linker such as glutaraldehyde. Glutaraldehyde reacts with primary amines to form an intersubunit link that locks the protein cage down and widens the range of temperature and pH stability. The result is a protein cage, 30 nm in exterior diameter and 24 nm in internal diameter, that is stable to the synthetic conditions necessary for the synthesis of γ -Fe₂O₃ nanoparticles (65°C and pH 8.5)⁷⁴. The particles synthesized in this manner are 18–19 nm in diameter and constrained within the protein cage architecture.

The magnetic properties of the synthesized nanoparticles are substantially different to those of γ -Fe₂O₃ nanoparticles synthesized in horse spleen ferritin and *Listeria Dps*. The blocking temperature for the 18.8 nm particles was found to

shift from 5 K or 30 K (*Listeria* Dps and ferritin, respectively) to 200 K (subE particles). Room-temperature hysteresis was observed with a coercive field of approximately 400 G. This shift is consistent with a larger particle size.

Other potential protein cages for the synthesis of magnetic nanoparticles

The sHsp from *Methanococcus jannaschii* (Mj) assembles into an empty 24-subunit cage with octahedral symmetry (Fig. 5)⁷⁵⁻⁷⁷. The assembled protein cage has an exterior diameter of 12 nm (Table 1). Large, 3 nm diameter pores at the three-fold axes allow free exchange between the interior and bulk solution⁷⁵⁻⁷⁷. In addition, the sHsp cage is stable up to 70°C and in a pH range of 5-11. Each 16.5 kDa Mj sHsp monomer is composed of 147 amino acids. In a reaction similar to ferritin, air oxidation of Fe(II) in the presence of sHsp leads to the formation of ferrihydrite⁷⁸ encapsulated within the sHsp protein cage, analogous to the ferritin reaction.

Lumazine synthase is a hollow 1 MDa bacterial enzyme of 60 β -subunits containing a core of three α -subunits⁷⁹ that is involved in the synthesis of lumazine, a precursor to riboflavin. The structure of lumazine synthase from *Bacillus subtilis* has been elucidated by X-ray crystallography. It has a hollow porous shell with icosahedral symmetry and inner and outer diameters of 7.8 nm and 14.7 nm, respectively (Table 1, Fig. 5)⁸⁰. The intersubunit contacts produce a cluster of three glutamic acid residues⁸⁰ and, because of the lack of compensating ligands, a region of negative charge density exists on the interior wall of the capsid, similar to the nucleation sites in ferritin. The interior of the lumazine synthase capsid is accessed through hydrophilic, funnel-shaped channels lined with glutamic acid residues, and located about the ten three-fold axes. The potential for lumazine synthase as a nanoreactor for iron oxide mineralization has been shown in the synthesis of lepidocrocite (γ -FeOOH).

Recent reports suggest that TMV is also useful as a template for nanomaterials synthesis⁸¹⁻⁸³. TMV is the prototypical tobamovirus that encapsulates a positive-sense RNA genome of 6.5 kb. The virion is a rigid rod of approximately 18 nm in diameter and 300 nm in length with a central hole 4 nm across (Table 1, Fig. 5). In addition, the virion is extraordinarily stable and can be manipulated under a variety of conditions. The 2130 identical coat protein subunits of 17.5 kDa are arranged in a right-handed helix with $16\frac{1}{3}$ subunits per turn⁸⁴. The exterior of the TMV

protein assembly provides a highly polar surface, which has been used successfully to initiate mineralization of iron oxyhydroxides, CdS, PbS, and SiO₂, as well as Au and Pt nanoparticles^{60,82}. Templated synthesis of Co and Ni metal nanowires inside TMV has also been reported^{85,86}, although magnetic properties have not yet been characterized.

Phage display techniques

In nature, organisms have evolved the ability to nucleate and assemble inorganic materials with almost perfect alignment, orientation, and shape using directed templating from organic matrices. As described earlier, biological systems control the nucleation, growth, and organization of mineral phases to create functional materials of iron oxide using vesicles to create a permanent magnetic dipole^{87,88}. These biological interactions can not only direct the nucleation of inorganic materials but also preferentially direct the growth of crystal type, face, and size, and can even control metastable crystalline forms^{89,90}. Nature has been limited to materials readily accessible in the environment. Peptide combinatorial library approaches allow for rapid selection and evolution of proteins for technologically important materials that nature has not yet had a chance to control.

Traditionally, peptide combinatorial libraries have been used in the selection of peptide sequences against organic targets by the pharmaceutical industry^{91,92}. Recently, phage display techniques have identified peptide sequences with high specificity toward particular inorganic materials⁹³⁻⁹⁹ and, in some cases, toward unique crystal faces¹⁰⁰. In this way, protein engineering, through directed evolution and screening of combinatorial peptide libraries using phage display, has identified peptide sequences with specific affinity toward inorganic materials not normally found under biological conditions. The screening of commercially available phage display libraries for binding to the ferromagnetic FePt and CoPt systems yielded a number of peptide sequences. In particular, the sequences HNKHPSTQPLA and CNAGDHANC for FePt and CoPt, respectively, were incorporated into the coat protein (gp8, where gp = gene product) of the M13 phage to provide a linear template that can simultaneously control inorganic particle phase and composition (Fig. 6)⁹⁷. The reduction of metal salt precursors in the presence of the gp8 modified phage yields coated particles that, when annealed at 350°C, give wires of CoPt and FePt in the L1₀ phase with uniform diameter (10 nm \pm 5%)⁹⁷.

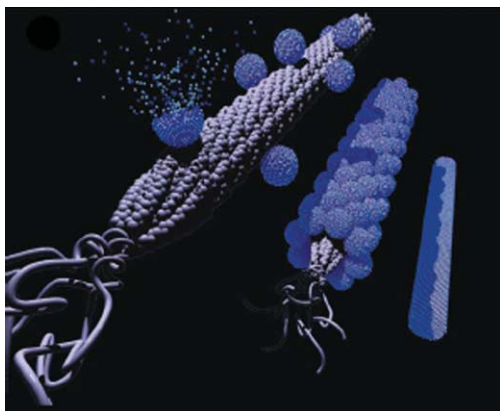


Fig. 6 Visualization of the M13 phage and the subsequent nanowire synthesis. The gp8 coat assembly structure is reconstructed from X-ray fiber crystallographic data (protein data bank number 1iff). The gp3 and gp9 proteins located at the proximal and remote ends of the virus, respectively, are not to scale and serve as representations of the proteins. The nanowire synthesis scheme is visualized for the nucleation, ordering, and annealing of virus-particle assemblies. (Reprinted with permission from⁹⁷. © 2005 Science.)

Magnetic measurements on the as-prepared FePt particles at 5 K and 300 K showed coercivities of 1350 G and 200 G, respectively¹⁰¹. The room-temperature coercivity was lower than that expected for samples containing only L1₀ FePt nanoparticles, but it demonstrates the existence of some high-anisotropy FePt nanoparticles. Synthesis of the FePt nanoparticles in the presence of M13 phage, in which the gp8 protein was modified to express a sequence unrelated to FePt, yields particles that lack the tetragonal distortion found in the L1₀ phase of FePt¹⁰¹.

Phage display and protein cages

Combining sequences obtained from phage display selection techniques with protein cage architectures allows synthesis of encapsulated magnetic nanoparticles under mild biomimetic conditions. This approach has recently been exploited in the synthesis of Ag inside ferritin¹⁰² and CoPt inside a genetically altered Mj sHsp¹⁰³.

Protein-engineered sHsp serves as a reaction vessel for the constrained synthesis of metallic CoPt nanoparticles. The spatially directed nucleation of CoPt particles displaying room-temperature ferromagnetism is achieved by coupling small peptide sequences to the cage-like architecture of Mj sHsp. Through site-directed mutagenesis, a small peptide sequence KTHEIHSPLLHK¹⁰¹ with a high specificity for the L1₀ phase of CoPt was introduced into the N terminus of the sHsp protein.

The purified Mj sHsp protein cages are treated with Co(II) and Pt(II) at pH = 8 and 65°C, and reduced by the addition of

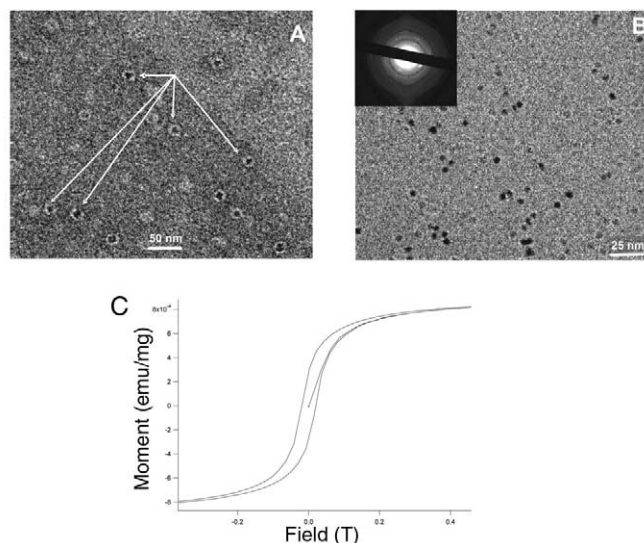


Fig. 7 (A) TEM of CoPt mineralized within a genetically altered heat shock protein (CP_Hsp) and negatively stained with 2% uranyl acetate. Arrows indicate protein cage/nanoparticle composites. (B) TEM of CoPt mineralized CP_Hsp with the electron diffraction pattern in the inset. (C) Hysteresis loop at 300 K for CoPt nanoparticles inside CP_Hsp with a coercive field of ~150 G.

excess NaBH₄ over 10 minutes. In the presence of the genetically modified sHsp, the reaction proceeded to form a homogeneous, charcoal-colored solution. The products of the reaction were imaged by transmission electron microscopy (TEM), and showed electron-dense cores with an average diameter of 6.5 ± 1.3 nm (Figs. 7A and 7B). When negatively stained with uranyl acetate, the metalized samples indicate that the protein cages remain intact and surround the metal cores. The CoPt particle diameters are consistent with the interior cavity dimensions of Mj sHsp. Electron diffraction indicates that the protein-encapsulated material is crystalline, and selected-area diffraction from a large number of particles reveals powder diffraction patterns with *d*-spacings consistent with the reported values of the L1₀ CoPt phase.

The CoPt nanoparticles encapsulated within genetically modified sHsp exhibit ferromagnetic behavior at room temperature, which is consistent with the L1₀ phase of CoPt. At 300 K, hysteresis in the magnetization curves is evident with a coercive field (H_c) of 150 G (Fig. 7C). The coercive field for this ferromagnetic component increased to 1100 G at 5 K. The saturation magnetization (M_s) of the annealed sample was determined to be ≈ 0.8 A m²/mg. Subsequent annealing of the sample at 650°C yielded a coercive field of 610 G. This data suggests that the specific peptide can initiate nucleation of the L1₀ CoPt phase, as indicated by the measured room-temperature ferromagnetism.

Applications of protein-encapsulated magnetic nanoparticles

Magnetic metallic alloys, such as the L1₀ phase of CoPt and FePt, for example, are of considerable interest as addressable bits for future use in magnetic storage applications because of their high magnetic anisotropy and chemical stability¹⁰⁷⁻¹¹². Ferritin has been used as a size-constrained reaction vessel for the growth of ferromagnetic CoPt nanoparticles¹⁰⁴⁻¹⁰⁶. The nanoparticles exhibit no distinct crystallinity or ferromagnetism at room temperature. After annealing, they become distinctly more crystalline, because of the loss of the protein shell as a result of heating. The nanoparticles are roughly spherical, with an average particle diameter of 4.1 nm and a standard deviation of 2.4 nm. The synthesized CoPt nanoparticles inside ferritin reveal no room-temperature ferromagnetism before annealing. Upon annealing, a coercive field of 300 Gauss is measured and sintering of the particles up to 25 nm in diameter is observed¹¹³.

The ability to produce self-assembled arrays of protein cages is of considerable interest for magnetic recording purposes (Fig. 8). Smooth particle films of CoPt in ferritin have been produced by spin coating or dip coating from aqueous solution. Recording densities of 1 Gb/cm² over 60% of the entire surface of a 65 mm glass disk substrate have been achieved. A maximum density of 2 Gb/cm² has been achieved on regions of the disk. The recording test shows that many particles are either at or below the superparamagnetic limit, but there are sufficient ferromagnetic grains to sustain large recording densities^{104,105}.

An approach to using ferritin as a cage-like host for molecular entrapment has recently been demonstrated¹¹⁴. A ferritin cage was disassembled under low-pH conditions and subsequently reassembled at almost neutral pH in the presence of the Gd-chelate complex GdDOTP (H8DOTP = 1, 4, 7, 10-tetrakis(methylenephosphonic acid)-1,4,7,10-

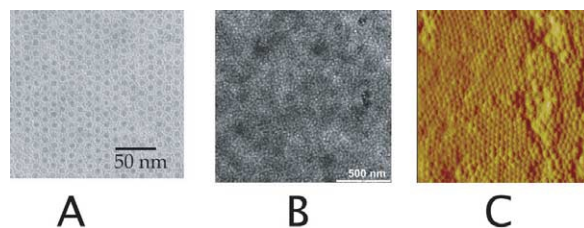


Fig. 8 Protein arrays obtained for (A) ferritin, (B) Dps from *Listeria*, and (C) CCMV on a polymer-coated Si substrate.

tetraazacyclododecane). This results in the entrapment of about 10 Gd-chelate complexes within the protein cage. This material has been shown to exhibit extremely high magnetic resonance imaging proton relaxivities, making it a promising candidate for applications in magnetic resonance imaging.

Summary

Biomimetic chemistry has evolved to a stage where ideas from molecular biology, protein chemistry, inorganic chemistry, and materials science can routinely be combined in the pursuit of novel materials. The use of protein cages for the synthesis of magnetic nanomaterials provides a number of unique advantages. Protein cages are biological in origin and, as such, are amenable to large-scale production. The cages can be modified routinely using either chemical or genetic approaches to impart specific chemical or structural functionality. Structural and functional plasticity allows many of the protein cage systems described to be engineered for specific applications in material science. The use of phage display libraries, based on a combinatorial library of random peptides, provides the potential to synthesize magnetic materials by targeted design. Also, the combination of peptide-mineral recognition with defined protein architectures holds promise for control over the morphology, composition, and properties of a wide range of future materials. **MT**

REFERENCES

1. Frankel, R. B., *et al.*, *J. Geophys. Res. B Solid Earth* (1998) **103** (B12), 30601
2. Blakemore, R., *Science* (1975) **190**, 377
3. Kirschvink, J. L. and Lowenstam, H. A., *Earth Planet. Sci. Lett.* (1979) **44** (2), 193
4. Lowenstam, H. A., *Science* (1967) **156**, 1373
5. Gider, S., *et al.*, *J. Appl. Phys.* (1996) **79** (8, part 2A), 5324
6. Mann, S., *J. Mater. Chem.* (1995) **5** (7), 935
7. Matsunaga, T., *et al.*, *J. Mater. Chem.* (2004) **14** (14), 2099
8. Lee, H., *et al.*, *Nano Lett.* (2004) **4** (5), 995
9. Arakaki, A., *et al.*, *J. Biol. Chem.* (2003) **278** (10), 8745
10. Philipse, A. P., and Maas, D., *Langmuir* (2002) **18** (25), 9977
11. Hanzlik, M., *et al.*, *J. Magn. Magn. Mater.* (2002) **248** (2), 258
12. Zablotskii, V., *et al.*, *J. Magn. Magn. Mater.* (2001) **234** (3), 575
13. Dunin-Borkowski, R. E., *et al.*, *Eur. J. Mineral.* (2001) **13** (4), 671
14. McCartney, M. R., *et al.*, *Eur. J. Mineral.* (2001) **13** (4), 685
15. Dunin-Borkowski, R. E., *et al.*, *Science* (1998) **282**, 1868

16. Pfutzner, H., *et al.*, *J. Appl. Phys.* (1991) **69** (8), 6024
17. Komeili, A., *et al.*, *Proc. Natl. Acad. Sci. USA* (2004) **101** (11), 3839
18. Rosenblatt, C., *et al.*, *Biophys. J.* (1982) **40**, 83
19. Frankel, R. B., and Blakemore, R. P., *J. Magn. Magn. Mater.* (1980) **15-18**, 1562
20. Bazylnski, D. A., *Int. Microbiol.* (1999) **2** (2), 71
21. Mann, S., *et al.*, *Nature* (1984) **310**, 405
22. Meldrum, F. C., *et al.*, *Proc. R. Soc. Lond. Ser. B-Biol. Sci.* (1993) **251** (1332), 231
23. Meldrum, F. C., *et al.*, *Proc. R. Soc. Lond. Ser. B-Biol. Sci.* (1993) **251** (1332), 237
24. Weiss, B. P., *et al.*, *Proc. Natl. Acad. Sci. USA* (2004) **101** (22), 8281
25. Matsuda, T., *et al.*, *Nature* (1983) **302**, 411
26. Mann, S. and Frankel, R. B., *Biom mineralization: Chemical and Biochemical Perspectives*, VCH, Weinheim, Germany, (1989), 389
27. Bazylnski, D. A. and Frankel, R. B., *Biom mineralization: Progress in Biology, Molecular Biology, and Application*, VCH, Weinheim, Germany, (2004), 17
28. Gorby, Y. A., *et al.*, *J. Bacteriol.* (1988) **170** (2), 834
29. Chasteen, N. D. and Harrison, P. M., *J. Struct. Biol.* (1999) **126** (3), 182
30. Harrison, P. M. and Arosio, P., *Biochim. Biophys. Acta-Bioenerg.* (1996) **1275** (3), 161
31. Jones, T., *et al.*, *Biochemistry* (1978) **17** (19), 4011
32. Harrison, P. M., *et al.*, *Adv. Inorg. Chem.* (1991) **36**, 449
33. Gider, S., *et al.*, *Science* (1995) **268**, 77
34. Gilles, C., *et al.*, *J. Magn. Magn. Mater.* (2002) **241** (2-3), 430
35. Gilles, C., *et al.*, *Eur. Phys. J. B* (2000) **17** (3), 417.
36. Kilcoyne, S. H., and Cywinski, R., *J. Magn. Magn. Mater.* (1995) **140-144** (part 2), 1466
37. Mann, S., *et al.*, *J. Mol. Biol.* (1986) **188** (2), 225
38. Towe, K. M., and Bradley, W. F., *J. Colloid Interface Sci.* (1967) **24** (3), 384
39. St. Pierre, T. G., *et al.*, *Inorg. Chem.* (1990) **29** (10), 1870
40. Moore, G. R., *et al.*, *J. Inorg. Biochem.* (1986) **28** (2-3), 329
41. St. Pierre, T. G., *et al.*, *Biochim. Biophys. Acta* (1986) **870** (1), 127
42. Lawson, D. M., *et al.*, *Nature* (1991) **349**, 541
43. Lawson, D. M., *et al.*, *FEBS Lett.* (1989) **254** (1-2), 207
44. Douglas, T., and Ripoll, D. R., *Protein Sci.* (1998) **7** (5), 1083
45. Xu, B. and Chasteen, N. D., *J. Biol. Chem.* (1991) **266** (30), 19965
46. Sun, S., and Chasteen, N. D., *J. Biol. Chem.* (1992) **267** (35), 25160
47. Douglas, T., *Biomimetic Synthesis of Nanoscale Particles in Organized Protein Cages*, VCH, New York, (1996), 91
48. Bulte, J. W. M., *et al.*, *Invest. Radiol.* (1994) **29**, S214
49. Bulte, J. W. M., *et al.*, *J. Magn. Reson. Imaging* (1994) **4**, 497
50. Meldrum, F. C., *et al.*, *Science* (1992) **257**, 522
51. Pankhurst, Q. A., *et al.*, *Hyperfine Interact.* (1994) **91**, 847
52. Wong, K. K. W., *et al.*, *Chem. Mater.* (1998) **10** (1), 279
53. Dickson, D. P. E., *et al.*, *Nanostruct. Mater.* (1997) **9**, 595
54. Resnick, D., *et al.*, *J. Appl. Phys.* (2004) **95** (11), 7127
55. Gilmore, K., *et al.*, *J. Appl. Phys.* (2005) **97** (10), 10B301
56. Gilmore, K., *et al.*, unpublished research
57. Mackle, P., *et al.*, *J. Am. Chem. Soc.* (1993) **115** (18), 8471
58. Mann, S., and Meldrum, F. C., *Adv. Mater.* (1991) **3** (6), 316
59. Meldrum, F. C., *et al.*, *J. Inorg. Biochem.* (1995) **58** (1), 59
60. Douglas, T., and Stark, V. T., *Inorg. Chem.* (2000) **39** (8), 1828
61. Resnick, D. A., *et al.*, *Phys. Rev. B* (2005), submitted
62. Grant, R. A., *et al.*, *Nat. Struct. Biol.* (1998) **5** (4), 294
63. Stefanini, S., *et al.*, *Biochem. J.* (1999) **338**, 71
64. Ilari, A., *et al.*, *Nat. Struct. Biol.* (2000) **7** (1), 38
65. Bozzi, M., *et al.*, *J. Biol. Chem.* (1997) **272** (6), 3259
66. Su, M. H., *et al.*, *Biochemistry* (2005) **44** (15), 5572
67. Allen, M., *et al.*, *Adv. Mater.* (2002) **14** (21), 1562
68. Yang, X. K., *et al.*, *Biochem. J.* (2000) **349**, 783
69. Allen, M., *et al.*, *Inorg. Chem.* (2003) **42** (20), 6300
70. Resnick, D., *et al.*, unpublished research
71. Speir, J. A., *et al.*, *Structure* (1995) **3** (1), 63
72. Douglas, T., and Young, M., *Nature* (1998) **393**, 152
73. Douglas, T., *et al.*, *Adv. Mater.* (2002) **14** (6), 415
74. Allen, M., *et al.*, unpublished research
75. Kim, K. K., *et al.*, *FASEB J.* (1998) **12**, A1329
76. Kim, K. K., *et al.*, *Nature* (1998) **394**, 595
77. Kim, R., *et al.*, *Proc. Natl. Acad. Sci. USA* (1998) **95** (16), 9129
78. Flenniken, M. L., *et al.*, *Nano Lett.* (2003) **3** (11), 1573
79. Schott, K., *et al.*, *J. Biol. Chem.* (1990) **265** (21), 12686
80. Ritsert, K., *et al.*, *J. Mol. Biol.* (1995) **253** (1), 151
81. Flynn, C. E., *et al.*, *Acta Mater.* (2003) **51** (19), 5867
82. Dujardin, E., *et al.*, *Nano Lett.* (2003) **3** (3), 413
83. Douglas, T., and Young, M., *Adv. Mater.* (1999) **11** (8), 679
84. Stubbs, G., *Philos. Trans. R. Soc. Lond. Ser. B-Biol. Sci.* (1999) **354** (1383), 551
85. Knez, M., *et al.*, *Nano Lett.* (2003) **3** (8), 1079
86. Knez, M., *et al.*, *Adv. Funct. Mater.* (2004) **14** (2), 116
87. Mann, S., (ed.) *Biomimetic Materials Chemistry*, Wiley-VCH, New York, (1996)
88. Mann, S., *et al.*, *Science* (1993) **261**, 1286
89. Belcher, A. M., *et al.*, *Nature* (1996) **381**, 56
90. Mann, S., *Angew. Chem. Int. Ed.* (2000) **39** (19), 3393
91. Smith, G. P., and Petrenko, V. A., *Chem. Rev.* (1997) **97** (2), 391
92. Benhar, I., *Biotechnol. Adv.* (2001) **19** (1), 1
93. Lee, S. W., *et al.*, *Science* (2002) **296**, 892
94. Whaley, S. R., *et al.*, *Nature* (2000) **405**, 665
95. Flynn, C. E., *et al.*, *J. Mater. Chem.* (2003) **13** (10), 2414
96. Seeman, N. C., and Belcher, A. M., *Proc. Natl. Acad. Sci. USA* (2002) **99**, 6451
97. Mao, C. B., *et al.*, *Science* (2004) **303**, 213
98. Sarikaya, M., *et al.*, *Nat. Mater.* (2003) **2** (9), 577
99. Naik, R. R., *et al.*, *Nat. Mater.* (2002) **1** (3), 169
100. McMillan, R. A., *et al.*, *Nat. Mater.* (2002) **1** (4), 247
101. Reiss, B. D., *et al.*, *Nano Lett.* (2004) **4** (6), 1127
102. Kramer, R. M., *et al.*, *J. Am. Chem. Soc.* (2004) **126** (41), 13282
103. Klem, M. T., *et al.*, *Adv. Funct. Mater.* (2005), in press
104. Hoinville, J., *et al.*, *J. Appl. Phys.* (2003) **93** (10), 7187
105. Mayes, E., *et al.*, *IEEE Trans. Magn.* (2003) **39** (2), 624
106. Warne, B., *et al.*, *IEEE Trans. Magn.* (2000) **36** (5), 3009
107. Christodoulides, J. A., *et al.*, *J. App. Phys.* (2000) **87** (9), 6938
108. Christodoulides, J. A., *et al.*, *IEEE Trans. Magn.* (2000) **36** (5), 2333
109. Ely, T. O., *et al.*, *J. Phys. Chem. B* (2000) **104** (4), 695
110. Sato, K., *et al.*, *Scripta Mater.* (2001) **44** (8-9), 1389
111. Stavroyiannis, S., *et al.*, *J. Appl. Phys.* (1999) **85** (8), 4304
112. Sun, S. H., *et al.*, *J. Phys. Chem. B* (2003) **107** (23), 5419
113. Mayes, E. L., and Mann, S., *Nanobiotechnology*, VCH, Weinheim, (2004)
114. Aime, S., *et al.*, *Angew. Chem., Int. Ed.* (2002) **41** (6), 1017
115. Simpson, E. T., *et al.*, *J. Phys. Conf. Ser.* (2005), in press